

The physical conditions in Gomez's Hamburger (IRAS 18059-3211), a pre-MS rotating disk

V. Bujarrabal¹, K. Young², and A. Castro-Carrizo³

¹ Observatorio Astronómico Nacional (OAN-IGN), Apartado 112, E-28803 Alcalá de Henares, Spain
e-mail: v.bujarrabal@oan.es

² Harvard-Smithsonian Center for Astrophysics, 60 Garden Street, Cambridge, MA 02138, USA
e-mail: rtm@cfa.harvard.edu

³ Institut de RadioAstronomie Millimétrique (IRAM), 300 rue de la Piscine, 38406 St. Martin d'Hères, France
e-mail: ccarrizo@iram.fr

Accepted

ABSTRACT

Aims. We aim to study the structure, dynamics and physical conditions of Gomez's Hamburger (IRAS 18059-3211; GoHam). We confirm that GoHam essentially consists of a flaring disk in keplerian rotation around a young, probably pre-MS star.

Methods. We present high resolution SMA maps of $^{12}\text{CO } J=2-1$, $^{13}\text{CO } J=2-1$, $^{12}\text{CO } J=3-2$, and $\text{C}^{17}\text{O } J=3-2$, as well as data on $^{12}\text{CO } J=6-5$ and the continuum flux at these wavelengths. Spatial resolutions up to $1''$ are obtained. Except for the C^{17}O data, the dynamical ranges are larger than 10. The maps are compared to a numerical model, which simulates the emission of a rotating disk with the expected general properties of such objects; a very satisfactory fitting of our maps is obtained. The meaning and reliability of our results are thoroughly discussed.

Results. Our observations allow measurement of the main properties of GoHam at scales between $\sim 1''$ ($\sim 5 \cdot 10^{15}$ cm, for the assumed distance, 300 pc) and the total extent of the nebula, $14''$. We are able to measure the global structure of the gas-rich disk, which is found to be flaring, and its dynamics, which is clearly dominated by keplerian rotation, with a very small degree of turbulence. The combination of different lines, particularly showing different opacities, allows us to reasonably estimate the distributions of the gas temperature and density. We clearly find a significant and sharp increase in temperature at large distances from the equator, accompanied by a decrease in density of the same order. Finally, we identify a condensation in the southern part of the disk that has no counterparts in the rest of the nebula. This condensation is quite extended (about $5 \cdot 10^{15}$ cm), contains a significant amount of mass (roughly, $\sim 6 \cdot 10^{-3} M_{\odot}$), and seems to be associated with a detectable distortion of the global rotation kinematics. We discuss several possible interpretations of that feature.

Key words. Stars: circumstellar matter – stars: protoplanetary disks – stars: formation – stars: individual: Gomez's Hamburger

1. Introduction

Gomez's Hamburger (IRAS 18059-3211; hereafter GoHam) is a very interesting nebula, originally identified on a plate by A. Gómez in 1985, that still remains poorly studied. It shows a spectacular optical image (see Ruiz et al. 1987; Bujarrabal et al. 2008, and HST images in press release number 2002-19), in which a dark lane of dust separates two flat, bright regions, presumably illuminated by a central star that remains hidden by the equatorial disk. The central star has been classified as an A0-type star, from spectroscopic analysis of the scattered light (Ruiz et al. 1987). GoHam's spectral energy distribution (SED) shows two maxima, in the optical and FIR (Ruiz et al. 1987), which respectively correspond to the stellar emission scattered by the bright lobes and to radiation reemitted by dust grains in the dark equatorial region.

Originally, GoHam was thought to be a post-AGB nebula (Ruiz et al. 1987). However, high-resolution CO maps (Bujarrabal et al. 2008, hereafter, Paper I) indicate that the nebula is almost exactly in keplerian rotation, around the symmetry axis clearly identified from its image. No component other than the rotating, flaring disk, at least at the large scale probed by the arcsec resolution attainable with mm-wave interferome-

try, seems to be present in the nebula. Bujarrabal et al. (2008) estimated the central (presumably stellar) mass and concluded that, for any possible distance, its high value in combination with the relatively low total luminosity of the source is not compatible at all with the idea that GoHam is an evolved object. These authors conclude that Gomez's Hamburger is very probably a pre-main-sequence object at a much smaller distance than previously believed, at about 500 pc. The value of the distance remains however uncertain. Wood et al. (2008) built a model for the dust emission and scattering that can explain the optical and IR SED for a distance of about 300 pc. The total disk mass determined by these authors, $0.3 M_{\odot}$, is very similar to that deduced in Paper I from a simple analysis of the mm-wave dust emission (taking into account the different distances assumed in these papers), and is very probably dominated by very dense inner regions. Recently, Berne et al. (2008) have also suggested a distance of about 200-300 pc, arguing that the spectral type could be slightly less early than that obtained by Ruiz et al. (1987). The determination of the distance is based on the comparison of several observational parameters obtained in GoHam with theoretical evolutionary tracks and previous data for other young stars. The relevant parameters are: the total luminosity (obtained from integration of the SED, but dependent on the anisotropy of the dust-processed radiation, see below) the central mass (from

Send offprint requests to: V. Bujarrabal

the nebula rotation), and the stellar surface temperature (see discussion on the stellar type accuracy by Berné et al.) If the stellar type is slightly less early than that proposed by Ruiz et al. (1987), a distance of about 300 pc is compatible with all existent data. These smaller values of the distance yield a slightly smaller linear radius for the disk, more in agreement with results usually found in similar objects. We accordingly adopt a distance of 300 pc.

The SED observations of GoHam are quite complete (Ruiz et al. 1987), but the estimate of the luminosity requires to introduce significant corrections due to the extreme viewing angle of the source and the strong disk opacity at short wavelengths (see Paper I). For the distance assumed here, we can expect a luminosity of $\sim 15 L_{\odot}$, with an uncertainty of about a factor 2. Comparison of this value of the luminosity with pre-MS evolutionary tracks (see van den Ancker et al. 1998, Paper I) indicates a stellar mass of about $2 M_{\odot}$. This value is relatively low compared to the mass derived from the disk rotation curve, $\sim 3 M_{\odot}$, suggesting a significant contribution to the central mass of the innermost disk or even of a low-mass stellar companion. See further discussion in Paper I; the nature of the central star(s) will be reviewed in Sect. 4, taking into account our new results.

Bujarrabal et al. (2008) presented only $^{12}\text{CO } J=2-1$ map obtained with the SMA, together with a preliminary modeling of the data. These models were severely hampered by the limited amount of data given in that work. In particular, the high optical depth expected in this line prevented any accurate determination of the gas density distribution. A significant revision of some parameters tentatively discussed by Bujarrabal et al. (2008) was therefore necessary. In this paper, we also present maps of $^{13}\text{CO } J=2-1$, $^{12}\text{CO } J=3-2$, and $\text{C}^{17}\text{O } J=3-2$. The combination of the $^{12}\text{CO } J=2-1$ line (reanalyzed for this work) with the ^{13}CO and C^{17}O lines, which are optically thin, and the $J=3-2$ emissions, requiring significantly more excitation, has allowed a very detailed modeling of the source. We think we can now propose realistic distributions at large scale of the gas density and temperature in Gomez's Hamburger, distributions that, as we will see, appear compatible with theoretical ideas on the properties of passive flaring disks in keplerian rotation.

2. Observations

We present observations of the $^{12}\text{CO } J=2-1$ (230.5 GHz), $^{13}\text{CO } J=2-1$ (220.4 GHz), $^{12}\text{CO } J=3-2$ (345.8 GHz), and $\text{C}^{17}\text{O } J=3-2$ (337.1 GHz) lines in Gomez's Hamburger (IRAS 18059-3211, GoHam), obtained with the Submillimeter Array (SMA). We also observed $^{12}\text{CO } J=6-5$ (691.5 GHz), but did not detect the line emission. ^{12}CO and $^{13}\text{CO } J=2-1$ were observed simultaneously in 2006. Details of the observations, calibration and data reduction for these lines may be found in Bujarrabal et al. (2008, Paper I). The $^{12}\text{CO } J=2-1$ data set has been reduced again, with respect to the observations presented in Paper I. The continuum flux at $\lambda = 1.3$ mm was measured to be 0.3 Jy.

The 345 GHz and 690 GHz data were taken on the night of 2007 March 21 (UT), when the array was in the "Compact North" configuration, a low resolution configuration with longer north-south baselines intended to produce nearly circular synthesized beams for low declination sources. Seven of the SMA's eight antennas were usable in the 345 GHz band, and six were usable in the 690 GHz band. The 345 GHz receivers were tuned to position the $^{12}\text{CO } J=3-2$ line at 345.796 GHz in the receivers' upper sideband (USB) and the $\text{C}^{17}\text{O } J=3-2$ line at 337.061 GHz in the lower sideband (LSB). The 690 GHz receivers were tuned to position $^{12}\text{CO } J=6-5$ at 691.473 GHz in the USB. The

J2000 coordinates used for GoHam were RA = 18:09:13.37, Dec = -32:10:49.5, and correspond to the central cross in our images. Observations began at 11:00 UT and finished at 21:10 UT. During that period, the precipitable water vapor above Mauna Kea varied from 0.6 to 1.0 mm. As the source transited at an elevation of 38 degrees, the double sideband (DSB) system temperature (T_{sys}) for the seven 345 GHz receivers ranged from 133 K to 235 K, while T_{sys} ranged from 1600 K to 2300 K for the 690 GHz receivers. The correlator was configured to have a uniform resolution of 812.5 kHz per channel across the full 2 GHz (DSB) bandpass of each receiver. This resolution is equivalent to 0.70 km s^{-1} for the $J=3-2$ lines, and 0.35 km s^{-1} for the $J=6-5$ line. Observations of Ganymede (16.5 degrees from the source) and the quasar 1924-292 (15.7 degrees from the source) were made every half hour for calibration of the instrument's complex gain. Saturn and 3C 273 were observed before the source rose, to provide bandpass calibration.

The data were calibrated with the MIR package. For the 345 GHz data, crosscorrelation observations of Saturn, 3C 273 and Ganymede were used to derive antenna-based bandpass data to correct for the instrument's spectral response. Ganymede was used for flux calibration, and the derived 850 micron flux for 1924-292 was 2.5 Jy. There were no phase jumps in the data, and complex gain calibration was done with a 5th order polynomial fit to the amplitude and phase of the quasar data. The source was tracked from an hour angle of -3.5 to +3.5 hours, and the total on-source integration time was 4 hours. Projected baseline lengths ranged from 9.1 to 136 kilolambda. The ^{12}CO and $\text{C}^{17}\text{O } J=3-2$ spectral lines were clearly detected, as was the 850 micron (345 GHz) continuum emission, with a total flux of 0.8 Jy. The astrometry was checked by using the Ganymede data to phase calibrate the 1924-292 data, and mapping 1924-292. The map showed 1924-292 as a point source with a position error of 0.2 arc seconds.

The 690 GHz band data were more difficult to process, in part because there were instrumental problems. Three of the correlator's 24 spectral bands were defective on some baselines. One receiver lost phase lock for 45 minutes during the track, and relocking the receiver produced a phase jump on baselines to that antenna. All data taken with $T_{\text{sys}} > 6000$ K (on either antenna of any baseline) were discarded. Finally, much of the data were taken after sunrise, when the pointing of the array antennas is degraded. The crosscorrelation amplitude of Ganymede was checked on all baselines, and the source data were discarded whenever the nearest (in time) Ganymede scans had low amplitudes. Altogether, roughly 1/3 of the 690 GHz data were discarded for these reasons. Saturn, 3C 273 and Ganymede again were used to provide instrument bandpass calibration. 1924-292 was not detected on short timescales in the 690 GHz data, so only Ganymede could be used for gain calibration. Ganymede was resolved by the array at 690 GHz, which caused the amplitude of this calibrator to pass through zero as the phase jumped by 180 degrees several times during the track. Projected baselines for the on-source data ranged from 17.9 to 230 kilolambda. The 450 micron (690 GHz) continuum emission from GoHam was detected, with a total flux of 1.5 Jy, but $\text{CO } J=6-5$ line emission was not, with a typical noise in the maps of ~ 1 Jy/beam.

Mapping was done with the NRAO AIPS package. The synthesized beam shapes were $3''.07 \times 1''.35$ with major axis position angle, PA = 37.4° for the $\text{C}^{17}\text{O } J=3-2$ maps, $2''.95 \times 1''.31$ with PA = 37.6° for the $^{12}\text{CO } J=3-2$ maps, and $3''.59 \times 0''.82$ with PA = -5.7° for the 450 micron continuum map.

The resulting maps per velocity channel of the four detected lines are shown in Figs. 1 to 5.

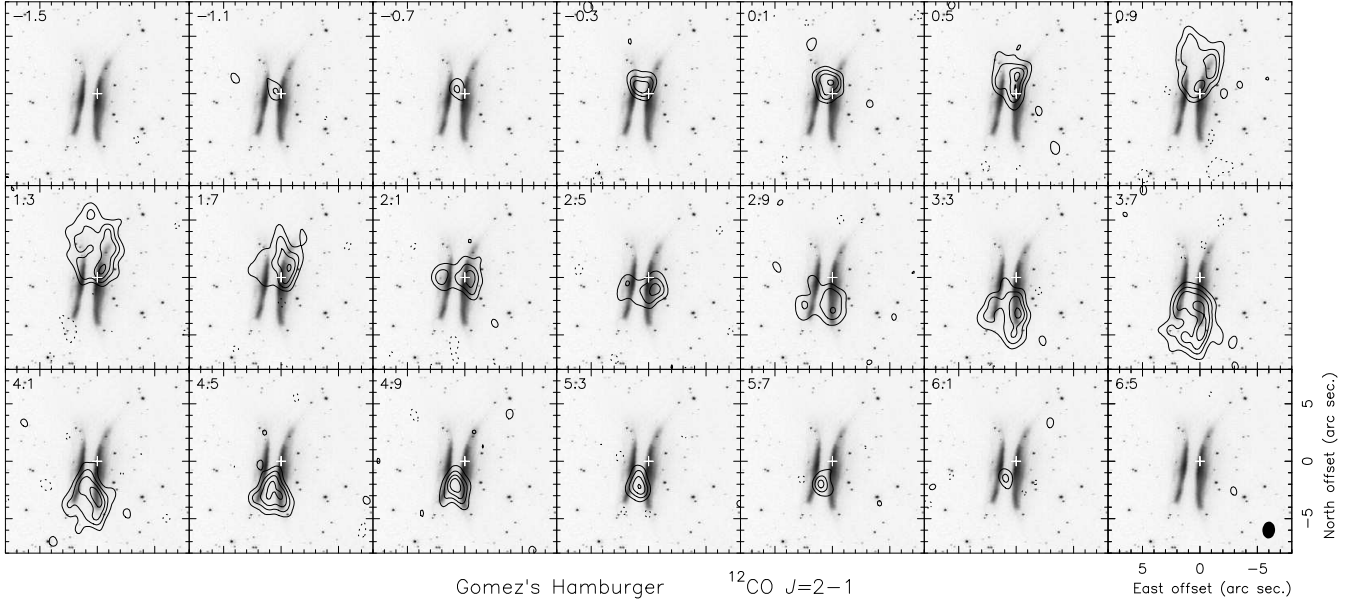


Fig. 1. Channel maps of the $^{12}\text{CO } J=2-1$ line from Gomez's Hamburger, continuum has been subtracted. First contour and contour step are 0.28 Jy/beam , approximately equal to 3σ ; negative values are represented by dashed contours. The LSR velocity in km s^{-1} for the center of each channel is indicated in the upper left corner. The J2000 coordinates of the reference position, the cross in the maps, are R.A. = 18:09:13.37, Dec = -32:10:49.5. In the last panel we represent the synthetic beam at half-intensity (black ellipse). The HST image is also shown for comparison. See details in Sect. 2.

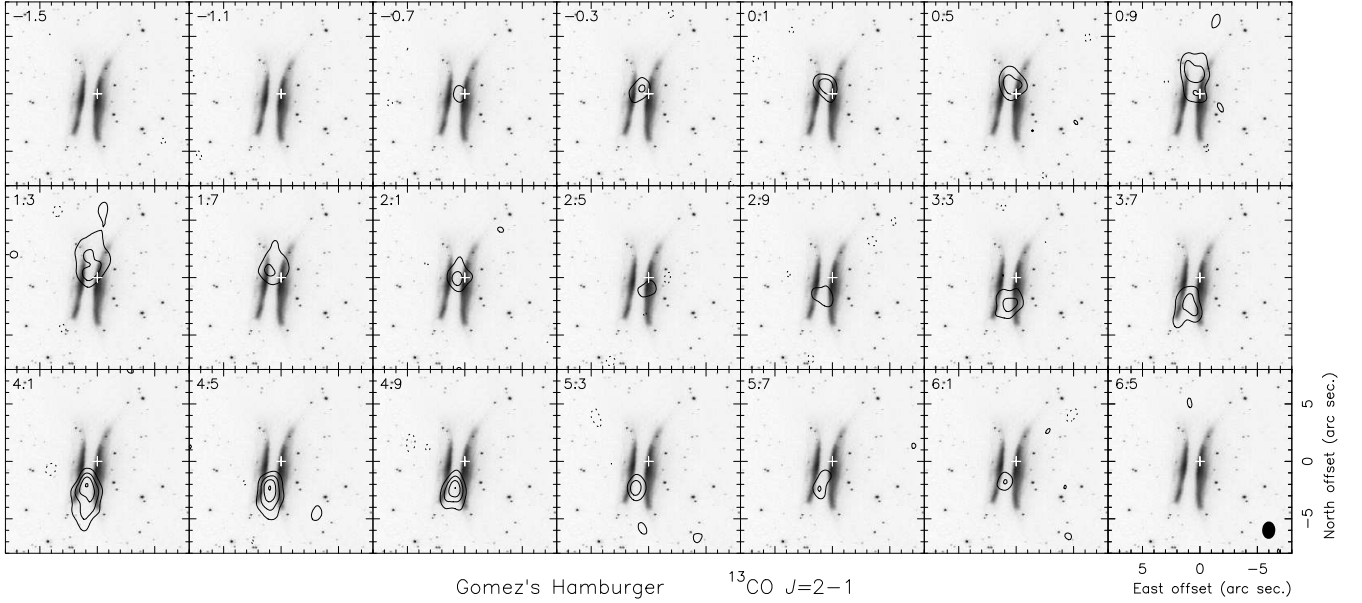


Fig. 2. Same as Fig. 1, but for the channel maps of the $^{13}\text{CO } J=2-1$ line observed from Gomez's Hamburger. First contour and contour step are also 0.28 Jy/beam .

In Figs. 1 and 2 we also represent the HST image of GoHam, to allow a better comparison with the CO emission and between both ^{12}CO and $^{13}\text{CO } J=2-1$ lines. In Fig. 3 we show a zoom of the data from Figs. 1 and 2 for the emission at velocities 0.9 and 4.1 km s^{-1} LSR, expected to represent the emission from regions closer to the plane of the sky. To show the HST images we have chosen the beautiful color image from press release 2002-19 provided by the HST newscenter (obtained from WFPC2 images, filters: F675W, F555W, F450W), see <http://hubblesite.org/newscenter/>. The coordinates were derived from the NICMOS images in the HST archive (taken on

April 12, 2006, HST project 10603, P.I.: D. Padgett; NICMOS images were more directly comparable to the press release image than the archive WFPC2 data). We have made use of the Aladin viewer and database. We recall that these images have not been yet published in the specialized literature and that a deep analysis of the HST imaging of GoHam is out of the scope of this paper.

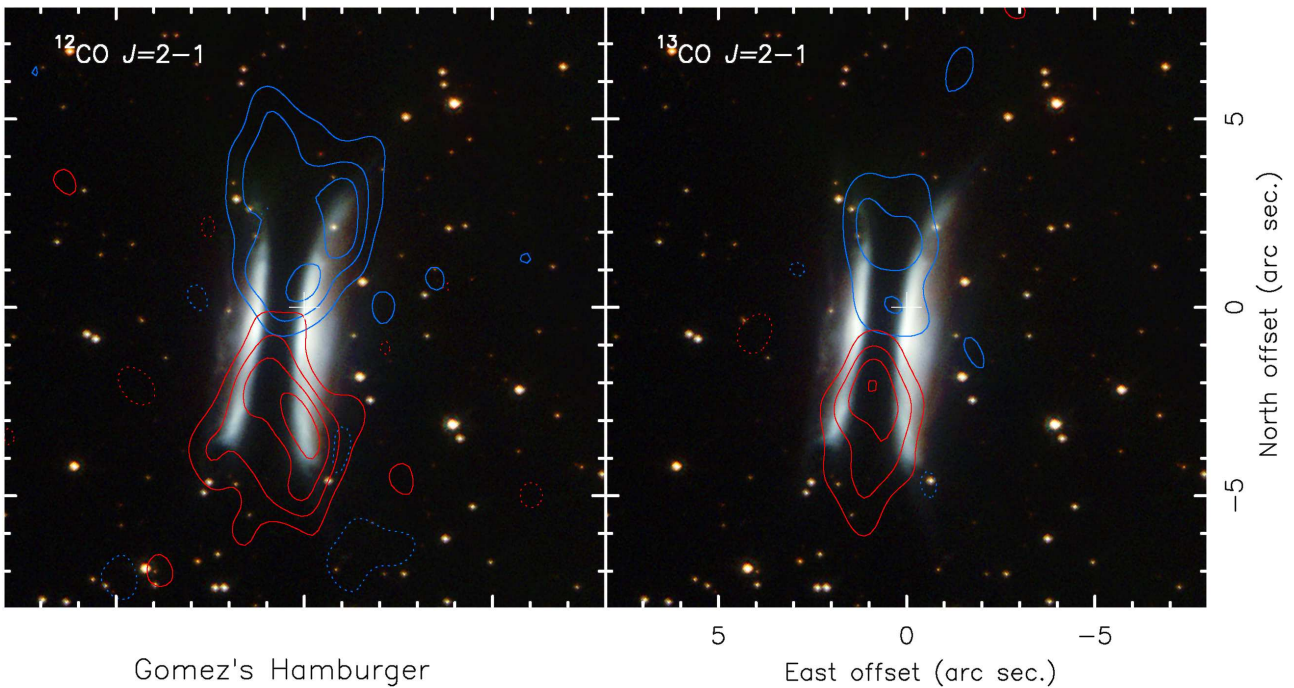


Fig. 3. Zoomed ^{12}CO and ^{13}CO $J=2-1$ emission for velocities 0.9 and 4.1 km s^{-1} , respectively blue (north) and red (south) contours, superposed to the HST image of GoHam; from Figs. 1 and 2, see further details in Sect. 2.

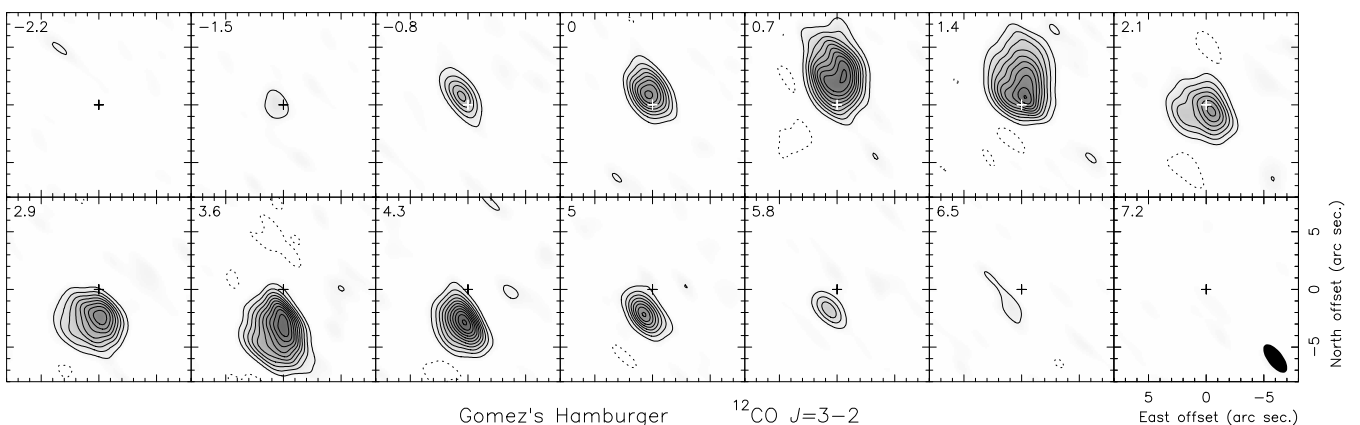


Fig. 4. Same as Fig. 1, but for the channel maps of the ^{12}CO $J=3-2$ line observed from Gomez’s Hamburger. First contour and contour step are 0.5 Jy/beam. Note that the spectral and spatial resolutions of these observations are somewhat poorer.

3. CO emission model

In order to extract as much information as possible from our maps, we have used a code that simulates the emission from a rotating model disk. Our model provides brightness distributions for LSR velocity channels, to be directly compared with the observations. We assume a shape of the CO cloud and a spatial distribution of the velocity, temperature, density, and CO relative abundance. Given these parameters, our code calculates the emissivity of the lines at each point of the disk, and the brightness for a number of lines of sight solving the full radiative transfer equation. Opacity effects and velocity shifts are accurately taken into account. Such a brightness distribution is convolved with the synthetic beam, and images with the same units as the observed ones are produced.

The code itself is similar to that described by Bujarrabal et al. (2008), Paper I. See further details there, including discussions on the basic assumptions. The method used to find the best fit

and the uncertainties in the derived parameter values are presented in the Appendix.

However, the disk model used here is much more complex than that in Paper I, mainly because the large amount of empirical data presented now allows us to undertake an accurate description of the structure and physical conditions in the disk. We have tried to reproduce all our SMA maps from the model predictions and, at the same time, to keep our disk model compatible as much as possible with theoretical ideas on the properties of rotating disks around young stars. As we will see in the next subsection, the model has become relatively complex, but the different disk components always correspond to features actually identified in our data.

3.1. Disk shape and dynamics

From a first inspection of our maps and the HST image (Figs. 1 to 3), it is clear that the nebula is essentially a rotating disk

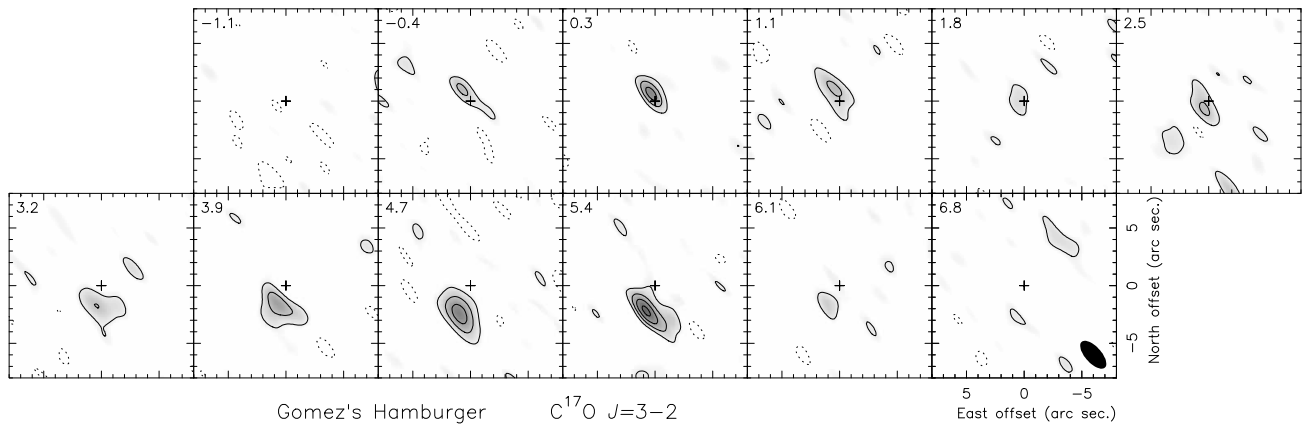


Fig. 5. Same as Fig. 3, but for the channel maps of the $C^{17}O$ $J=3-2$ line observed from Gomez's Hamburger. First contour and contour step are 0.3 Jy/beam.

seen almost edge on, with a significant axial symmetry and almost exactly keplerian dynamics. We can also see that the disk is roughly flaring, being significantly wider at larger distances from the center. The disk symmetry axis is almost placed in the plane of the sky, slightly tilted such that the western part of the disk points towards us. The projection of the disk symmetry axis on the sky plane is almost in the east-west direction, with position angle, $PA \sim 85^\circ$, i.e. the disk appears almost parallel to the declination axis.

We accordingly assume that the emission comes from a flaring disk in keplerian rotation and showing axial symmetry. Our calculations confirm that the observations can be explained under these assumptions. Two dimensions are then enough, r , the distance to the disk axis, and z , the distance to the disk equator.

We assume the simplest flaring geometry, with a disk width just proportional to r . Note that, in our case, the disk boundaries represent the region where CO is still abundant, before it is significantly photodissociated (due to the UV radiation from the central star or from the galactic background), although the comparison of the ^{12}CO maps with the HST scattered light images (Figs. 1 to 3) suggests that the ^{12}CO disk in fact occupies the whole nebula. To keep the model as simple as possible, we assume constant CO abundance, $X(CO)$, and isotopic ratios. Note that the CO abundances and density laws are not independent parameters in our model; therefore, the value of $X(^{12}CO)$ given here is in fact an assumption chosen to be reasonably in agreement with expectations. We recall that the molecular abundances in inner regions of the disk may be significantly smaller than the usual ones in the interstellar medium, mainly due to depletion onto grains (see discussion in e.g. Panić et al. 2008; Thi et al. 2004, and references therein). As mentioned above, in the outer regions of the disk we could expect significant dissociation of CO. We must therefore keep in mind that, although the CO abundance assumed here for ^{12}CO , 10^{-4} , is moderate, its value could be still lower in the innermost regions.

As we can see in our ^{12}CO $J=2-1$ maps, particularly at 1.3 $km\ s^{-1}$ LSR, the shape of the outer part of the disk seems to be rounded, instead of flaring (at large distances, $r > R_m$, to the center). The model predictions are very clearly different from the observations if we assume that the flaring geometry continues up to the outer disk radius. This assumption is compatible with calculations of the shape of the CO abundance variations at large values of r , see e.g. Jonkheid et al. (2006, 2007). We will see from our model calculations how this disk shape well reproduces the observations. The shape of the disk is then given by

the following parameters: The outer maximum and inner minimum disk radii, R_{out} and R_{in} ; the intermediate radius up to which the disk is flaring, R_m ; and the width at a given value of r , $H(r_0)$, such that $R_{in} \leq r_0 \leq R_m$. Between R_m and R_{out} , the disk width is assumed to vary following an elliptical function. See the resulting disk shape in Fig. 7.

The kinematics is assumed to be given by the rotational velocity, following a keplerian law with r , i.e. varying proportionally to $1/\sqrt{r}$. As in paper I, we find that some amount of local turbulent dispersion helps to fit the data, but that its value must be kept very small. We then assume the existence of a constant local dispersion V_{turb} .

3.2. Density and temperature

Direct inspection of our data suggests that the density and temperature distribution must follow relatively complex laws, that we will introduce in our model, trying to keep them compatible with general theoretical ideas.

We can see, first of all, a remarkable difference between the ^{12}CO and ^{13}CO $J=2-1$ maps, see Figs. 1 and 2 and a zoom of intermediate velocities in Fig. 3. The ^{13}CO brightness distribution is significantly narrower (less extended in the direction of the disk axis, which is almost equivalent to the east-west direction) and shorter (less extended in the disk plane direction). Nevertheless, in regions in which both lines are intense (in the disk plane, slightly northwards and southwards from the star), the ^{12}CO $J=2-1$ brightness is only slightly higher. On the other hand, in the disk edges, where only ^{12}CO emission appears, the brightness of this line is often significantly higher than in the central regions (where both $J=2-1$ transitions are detected).

Since ^{13}CO emission is certainly expected to be much less optically thick than ^{12}CO emission and both lines are easily thermalized, this different behavior between them obviously means that there are wide outer edges of the disk in which the density significantly decreases and the temperature increases. These edges are both more or less parallel to the disk equator (appearing from certain values of $|z|$) and perpendicular to it (appearing from certain values of r). This behavior is very noticeable in the direction perpendicular to the plane, i.e. sharp variations of density and temperature take place from a certain distance to the disk equator, and are particularly well identified in the maps. We can also see in our ^{12}CO $J=2-1$ maps that one of these edges parallel to the equator (so, almost parallel to the north-south direction), the western one, is significantly more intense than the other. This

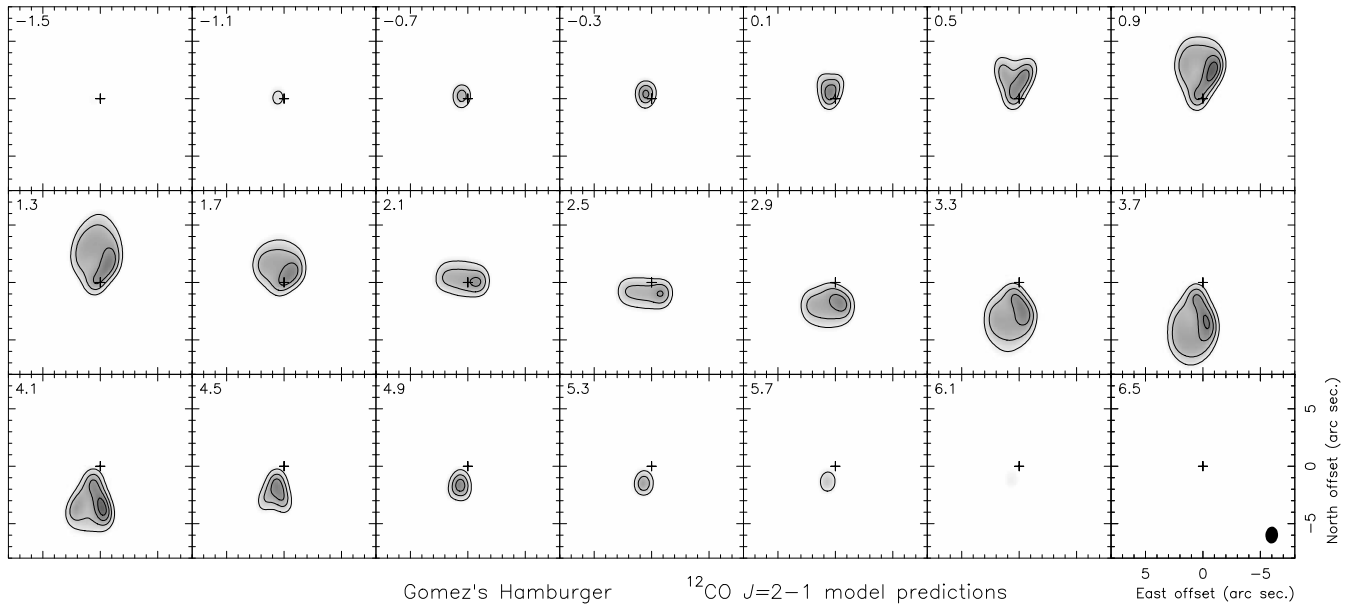


Fig. 6. Predictions of the $^{12}\text{CO } J=2-1$ line brightness from our best model fitting for the GoHam disk. The spatial scale and contours are the same as in the observations, Fig. 1.

is due to a simple radiative transfer effect: the emission from the eastern edge is absorbed by the cooler and opaque inner regions, which does not occur for the emission from the other side, which is closer to us. As we will see, our model reproduces very convincingly this phenomenon. Of course, nothing comparable is seen in the optically thinner ^{13}CO emission, which, because of the low density of the hot edges, is only intense in the dense central regions.

Therefore, to reproduce the observations of the different lines, we have to introduce several components in our density and temperature laws. At a minimum we need a cool dense region close to the equator, plus two edges with significantly less density and higher temperature (which are more or less parallel to the equator and separated quite sharply from the previous equatorial region), plus an outer region far from the disk axis with similar but smaller variations in these parameters.

We finally introduce a new correction: to explain the relatively intense emission for regions close to the central star, in spite of their small volume in a flaring disk, the density and temperature must increase from the standard values at small enough distances from the star. As we will discuss in the Appendix, the physical properties of these regions, unresolved in our observations, are not well determined.

The equatorial density and temperature (n_{eq} , T_{eq}) are supposed to follow potential laws, $n_{\text{eq}}(r) \propto 1/r^{\alpha_n}$ and $T_{\text{eq}}(r) \propto 1/r^{\alpha_T}$. Such laws are often found to be compatible with studies of molecular gas in disks around young stars (e.g. Dutrey et al. 2007), and we find that these simple laws are enough for the amount of information actually contained in our data. In practice, we assume that α_n is not a free parameter but equal to 1, a value that can fit our results. Note that the assumption of constant accretion rate, sometimes assumed to derive the density law, can hardly be justified in a relatively evolved object like GoHam, whose central star is barely accreting material.

The variation of the density with z , the distance to the equator is assumed to be given by the vertical equation of hydrostatics (see e.g. Dullemond et al. 2007):

$$\frac{dP}{dz} = -\rho \Omega^2 z. \quad (1)$$

Where the pressure is $P = kT/m_p$, m_p is the average weight of the gas particles, ρ is the density, and $\Omega(r)$ is the angular velocity.

For a constant temperature with z , $T(r, z) = T_{\text{eq}}(r)$, $n(r, z)$ is given by:

$$n(r, z) = n_{\text{eq}}(r) e^{-\left(\frac{z^2}{2T_{\text{eq}}(r)}\right)}. \quad (2)$$

Where $C_1 = \Omega^2(r) m_p/k$ is a function of r , not of z .

To implement the above mentioned sharp change in temperature and density from a value of $|z|$, we assume that when $n(r, z)$ reaches a certain fraction of $n_{\text{eq}}(r)$ the temperature changes by a factor, F_T . The value of F_T is obtained from comparison between the observations and the model predictions, see Table 1 and Sect. 4, as well as the fraction of the density at which the jump must appear (1/10 was found to yield acceptable model results).

We are assuming that there is also a jump of the density at this point, by a factor F_n . F_n can be calculated from the equation of hydrostatics, which can be written in the form:

$$\frac{1}{\rho} \frac{dP}{dz} = -\frac{z C_1}{T} - \frac{1}{T} \frac{dT}{dz}. \quad (3)$$

For a very steep jump in T:

$$\frac{1}{\rho} \frac{dP}{dz} \sim -\frac{1}{T} \frac{dT}{dz}. \quad (4)$$

Whose solution, for a jump between T_0 and T_1 , is:

$$\frac{\rho_1}{\rho_0} \sim \frac{T_0}{T_1}. \quad (5)$$

So, if the temperature varies at a given value of z , z_j , by a factor F_T , the density must vary at the same point by a factor $F_n = 1/F_T$. Beyond this point, for $z \geq z_j$, we assume that the temperature remains constant, and then the density must continue the law already deduced for constant temperature:

$$n(r, z) = n(r, z_j) e^{-\left[\frac{(z-z_j)^2}{2T(r, z_j)}\right]}. \quad (6)$$

Where $z > z_j$ and $n(r, z_j)$ and $T(r, z_j)$ denote the density and temperature just beyond the jump at z_j .

We note that, for the law we are assuming for $n_{\text{eq}}(r)$ ($n_{\text{eq}}(r) \propto 1/r$), the condition for the jump we are imposing, i.e. that $n(r, z)/n_{\text{eq}}(r)$ is smaller than a certain constant factor, is roughly equivalent to assume that the jump appears for a fringe roughly parallel to the outer limit of the CO-rich disk in z . This is reasonable, since both the photodissociation of CO and the gas over-heating are expected to be physically due to the effects of the outer radiation field.

We have also mentioned that T and n must also depart from our standard law in the outer disk, for $R_m < r < R_{\text{out}}$; again, n must show a decrease and T must increase to explain the ^{12}CO and $^{13}\text{CO } J=2-1$ emission from regions far from the symmetry axis. The n and T variations are assumed to be not related in this case. See the finally adopted laws in Table 1 and Fig. 7. Note that the required change in T is small, but n must strongly decrease to explain the lack of ^{13}CO emission (and the decrease of the $^{12}\text{CO } J=2-1$ intensity close to R_{out}). In any case, the accuracy of the density value determined at the longest distances from the axis is poor, since it mostly depends on the intensity of only one line, which is (moderately) optically thick; see Appendix. Note that, for the adopted physical conditions, the density in regions with r slightly larger than R_m is high enough to allow detectable emission of ^{13}CO and $^{12}\text{CO } J=2-1$ for some LSR velocities. The central velocities of our $^{12}\text{CO } J=2-1$ maps are affected even by the outermost parts of the disk.

3.3. Other parameters

The inclination of the rotation axis with respect to the plane of the sky must be small, as suggested by the optical and CO images. The projection of this axis on the plane of the sky is obviously placed at position angle, PA, slightly smaller than 90° . We note that both parameters may in fact vary with r , since such a big disk may be warped at some degree. This seems to be the case if we compare the inclinations in the CO maps for $V_{\text{LSR}} \sim 1.3-1.7 \text{ km s}^{-1}$ and for 0.9 or 3.3 km s^{-1} . It is probable that some regions of the disk rotate around an axis (in projection) at PA $\sim 80^\circ$, while other regions rotate around PA $\sim 90^\circ$.

The distance has been discussed in Paper I and Sect. 1, where the uncertainties of its value were stressed. We adopt a distance of 300 pc.

The systemic velocity is determined from the maps of our CO lines, it is quite accurately measured, with an accuracy better than a 10%. The given value, Table 1, is compatible with all the observations presented here.

3.4. Fitting procedure and results

We have chosen the best set of parameters by direct comparison of the observed and synthetic images. We think that the comparison in the sky plane, and not in the transformed uv plane, is possible in our case because of the relatively large extent of the source. On the other hand, the large number of parameters, needed to explain the various components suggested by the observational features, and the different significance of them, prevents any systematic, blind fitting. See detailed discussion in App. A.1. The ^{12}CO and $^{13}\text{CO } J=2-1$ images, which contain a lot of information, have been the basic data for this comparison.

In the Appendix we can also see in detail the criteria followed to choose the acceptable models. The residual images, i.e. the observed minus theoretical images, must present an r.m.s.

noise in regions where emission appears smaller than ~ 1.5 times that found in nearby regions (that just gives the noise of the observations). Also, the residual images must show contours smaller than ~ 3 times the noise level or ~ 2 times systematically. For instance, for a model to be acceptable, we must not see in the resulting $^{12}\text{CO } J=2-1$ residuals two positive or negative contours; note that the observed $^{12}\text{CO } J=2-1$ image do show one contour features just due to the observational noise. For an acceptable model, the regions in the residual images in which emission was present appear, therefore, only slightly different from those in which there was no emission.

We have discussed in A.2 the uncertainty in the main parameters of the model, given by the values of each parameter that, while the others remain unchanged, lead to results that clearly do not satisfy these conditions.

The conditions for the model predictions to be acceptable are somewhat relaxed for the relatively strong emission detected at about $4.5-5.5 \text{ km s}^{-1}$, which has no counterpart in the equivalent blueshifted emission. We think that this emission excess is due to a condensation in the rotating gas (Sect. 4 and App. A.3). Our model presents axial symmetry and cannot reproduce this emission excess; we have preferred to fit mostly the emission in the other velocities and to discuss separately this intense clump (Sect. 4.1).

We present in Fig. 6 and in the Appendix some examples of the resulting model maps and residuals. Table 1 and Fig. 7 present the values of the fitted parameters.

4. Results and conclusions

Our SMA observations of $^{12}\text{CO } J=2-1$, $^{13}\text{CO } J=2-1$, $^{12}\text{CO } J=3-2$, and $\text{C}^{17}\text{O } J=3-2$ in Gomez's Hamburger (Sect. 2, Figs. 1 to 5) have yielded high-quality, gorgeous maps. The maps have been satisfactorily reproduced by our model of disk in keplerian rotation (see Sect. 3, Fig. 6, A.2). From these maps, taking into account our model fitting of the data and even directly from them (see Sect. 3), we have been able to derive the main structure, dynamics and physical conditions of the nebula. See parameters of the model and best fitting in Sect. 3, Fig. 7, and Table 1. We assume a distance of 300 pc, see Bujarrabal et al. (2008, Paper I) and Sect. 1, the dependence of the fitting on the distance is given in Table 1. See further discussion on the fitting procedures and accuracy in the Appendix.

The CO emitting gas in GoHam forms a rotating disk that is probably quite coincident with the whole nebula, since the CO extent is even larger than the HST image (showing scattered light and absorption by dust grains, see Figs. 1 to 3). We recall, however, that the disk shape given here is in fact that of the region in which CO is rich. Other nebula components in which molecules are severely underabundant, due to photodissociation by the interstellar or stellar UV field or to depletion onto grains, are not probed by our maps.

Our data confirm the previous conclusion (Paper I) that the disk is very nearly in keplerian rotation and shows a clear axial symmetry. However, we detect, mainly from $^{13}\text{CO } J=2-1$ maps (Figs. 2, 3) and their comparison with the model predictions, that there is a condensation in the southern disk that has no counterpart in the rest of the nebula; see discussion on its properties and meaning in 4.1.

The general dynamics and structure of the nebula are relatively well determined from the maps. We note that the shape of the model disk essentially corresponds to the region in which, due to shielding from the external UV field, CO is still abundant.

Table 1. Structure and physical conditions in the molecular disk in Gomez's Hamburger, derived from our model fitting of several CO rotational lines. Dependence on the assumed distance is given in the relevant cases. Other parameters of the modeling are also given.

Parameter	Law	Values	comments
Outer radius		$R_{\text{out}} = 3.1 \cdot 10^{16} \left(\frac{D(\text{pc})}{300}\right) \text{ cm}$	
Intermediate radius		$R_{\text{m}} = 1.7 \cdot 10^{16} \left(\frac{D(\text{pc})}{300}\right) \text{ cm}$	
Inner radius		$R_{\text{in}} = 3 \cdot 10^{15} \left(\frac{D(\text{pc})}{300}\right) \text{ cm}$	
Disk thickness	linear	$H(10^{16} \text{ cm}) = 9.5 \cdot 10^{15} \text{ cm}$	
Tangential velocity	$V_t \propto 1/\sqrt{r}$ (keplerian)	$V_t(10^{16} \frac{D(\text{pc})}{300} \text{ cm}) = 2.1 \text{ km s}^{-1}$ central mass: $3 \left(\frac{D(\text{pc})}{300}\right) M_{\odot}$	
Temperature (equator) see text and Fig. 7	$T_{\text{eq}} \propto 1/r^{\alpha_T}$	$T_{\text{eq}}(10^{16} \frac{D(\text{pc})}{300} \text{ cm}) = 16 \text{ K}$ $\alpha_T = 0.3$	+ increase in the edges, by a factor 3 + increase beyond R_{m} , $T(R_{\text{out}}) = 17 \text{ K}$ + increase within $2 \times R_{\text{in}}$, by a factor of 2
Gas density (equator) see text and Fig. 7	$n_{\text{eq}} \propto 1/r^{\alpha_n}$	$n_{\text{eq}}(10^{16} \frac{D(\text{pc})}{300} \text{ cm}) = 1.5 \cdot 10^6 \left(\frac{300}{D(\text{pc})}\right) \text{ cm}^{-3}$ $\alpha_n = 1$	+ decrease with z , following hydrostatic eq. + decrease beyond R_{m} , $n_{\text{eq}}(R_{\text{out}}) = 1000 \text{ cm}^{-3}$ + increase within $2 \times R_{\text{in}}$, by a factor of 2
Relative abundances	constant	$X(^{12}\text{CO}) : X(^{13}\text{CO}) : X(\text{C}^{17}\text{O}) = 10^{-4} : 1.5 \cdot 10^{-6} : 2 \cdot 10^{-7}$	assumed value for $X(^{12}\text{CO})$

Other parameters	Values	comments
Axis inclination from the plane of the sky	6°	from optical and CO data
Axis inclination in the plane of the sky (PA)	85°	from optical and CO data
Distance	300 pc	from luminosity and mass values (Sect. 1)
LSR systemic velocity	2.5 km s^{-1}	from CO data

The shape we deduce is compatible with the general structure expected for the CO-rich parts of disks around young stars, see e.g. Jonkheid et al. (2006, 2007).

The distributions in the model of the number density (n) and temperature (T) require a deeper discussion. The difference between the distributions of ^{12}CO and ^{13}CO $J=2-1$ emission is particularly useful for such a purpose. The bright rims, more or less parallel to the equator, clearly seen in the optically thick

^{12}CO emission are not present in ^{13}CO . Since ^{13}CO $J=2-1$ is certainly much less opaque than ^{12}CO $J=2-1$, this indicates a significant increase in temperature and decrease in density in regions sufficiently separated from the equator. We note that this decrease of the density with the distance to the equator, z , appears in our model as a result of the jump in temperature, since the variation of the density with z is assumed to be just given by the equation of hydrostatics for a rotating disk. Our model re-

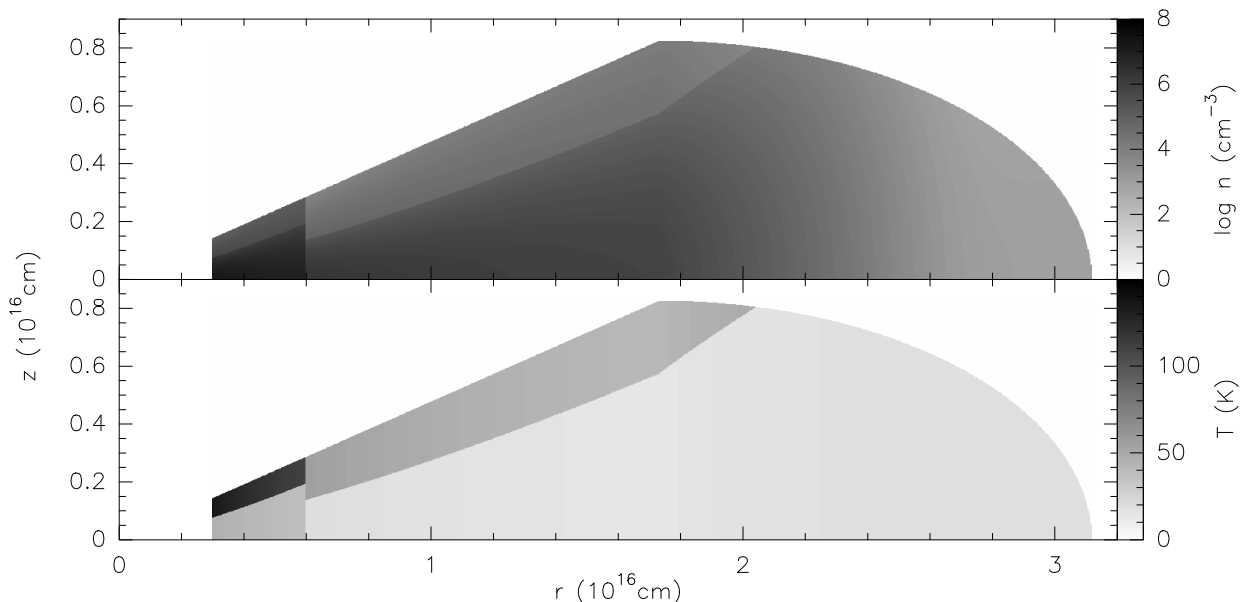


Fig. 7. Density and temperature distributions in our best-fit model. r is the distance from the rotation axis, and z is the distance to the equator.

produces the observations assuming a characteristic (sharp) increase of the temperature by a factor 3. We note that the ^{13}CO $J=2-1$ emission comes quite accurately from the opaque equatorial disk seen in the HST images (Figs. 2, 3), while the bright rims detected in ^{12}CO $J=2-1$ at large distances from the equator correspond to the flaring-disk edge that appears in the visible and NIR as a result of the scattering of stellar light by dust (Figs. 1, 3).

Similar changes in the physical conditions within the disk have been predicted from theoretical considerations (see e.g. Dullemond et al. 2007). Some previous maps of disks around young stars have also suggested an increase in temperature of this order (e.g. Dartois et al. 2003).

Comparison of the ^{12}CO and ^{13}CO maps also suggests that n decreases and T increases at large distances to the center in the plane (large values of r), in view of the significantly less extended emission of ^{13}CO $J=2-1$ and the relative maxima found in ^{12}CO $J=2-1$ at such large distances. In this case the variations of the temperature and density are assumed to be independent, indeed we find that the density decrease factor must be larger. A general description of the spatial distribution of the physical conditions can be seen in Fig. 7. We recall that we are assuming that the molecular abundances are constant within the whole disk, because the existent data do not allow to consider independently variations of the abundances together with variations of the density and temperature. Therefore, the decrease in density for large r could (at least partially) reflect a decrease of the ^{13}CO abundance in those regions. (This does not affect the rest of our conclusions: the temperature must increase for high values of z and of r , to explain the higher ^{12}CO intensity, and the density for high z must decrease to satisfy the hydrostatics equations.)

A clear asymmetry is seen in the ^{12}CO brightness distribution with respect to the disk equator, i.e. between the eastern and western parts of the nebula. This effect is due to self absorption: the cold equator absorbs the emission coming from the hot, outer regions at high z that are placed behind it (corresponding to the east part of the CO image), which of course does not affect the emission of the hot layer that is closer to us. This asymmetry is very well reproduced by our model calculations, which accu-

ately take into account opacity effects and radiative interactions between the different parts of the nebula.

We note the very low degree of local turbulence deduced from the model fitting, $\lesssim 0.1 \text{ km s}^{-1}$. Very small values of the microturbulence velocity are often found in rotating disks (e.g. Panić et al. 2008), even in the rare cases of disks rotating around evolved stars (Bujarrabal et al. 2005).

The total central mass responsible for the observed rotation is deduced to be $\sim 3 M_{\odot}$. We have seen in Sect. 1 and Paper I that this mass value seems somewhat high compared to that derived from the comparison of the total luminosity with evolutionary tracks, $\sim 2 M_{\odot}$ (with high uncertainties). As we discussed in Paper I and Sect. 1, this value may include as much as $\sim 0.5 M_{\odot}$ due to the mass of very dense and very inner regions of the disk (not well probed by our observations, which do not attain the required very high resolution). Therefore, the comparison of the mass values derived from the evolutionary tracks and from the disk dynamics may still imply the presence of a binary star in GoHam. The conclusion on the binary nature of the central star depends, unfortunately, on the comparison of theoretical evolutionary tracks with the uncertain values of the stellar luminosity and surface temperature, values that cannot at present be determined with enough accuracy (see Paper I and Sect. 1).

Our model also gives the total mass of the (extended) disk. From integration of the model density, we find a value of $\sim 0.01 M_{\odot}$. As in our previous work (Paper I), we find a disk mass value much smaller than the total mass derived from dust emission ($\sim 0.3 M_{\odot}$; Sects. 1, 3). This may be due to a strong gas depletion onto grains, mainly in the densest regions of the disk (Dutrey et al. 1997; Thi et al. 2004; Panić et al. 2008), which could yield a higher dust mass and lower molecular abundances than expected. We think that this effect could at least partially explain the discrepancy found between the mass derived from dust emission and from CO maps. Unfortunately, dust continuum emission has been found to come dominantly from the very center of the disk, which is poorly mapped in our $1''$ -resolution CO line maps, avoiding a proper comparison of both distributions. A future study of the effects of depletion on the mass determinations in this source will require significantly deeper maps of

the continuum emission, tracing dust up to distances comparable to those observed in CO emission, as well as higher resolution maps of CO lines, accurately mapping the inner disk regions.

4.1. The southern condensation

As we have discussed in Sect. 3, there is an asymmetry in our data, particularly in the $^{13}\text{CO } J=2-1$ maps, that cannot be accounted for by an axially symmetric model (Figs. 2, 3). We can see an emission excess in the southern part of the nebula, at about $1''.3$ from the nebula center ($6 \cdot 10^{15}$ cm for the assumed distance of GoHam) and between about $+4.5$ and $+5.5 \text{ km s}^{-1}$ LSR, which has no counterpart in the corresponding northern emission at more negative velocities. This asymmetry cannot be due to opacity or excitation effects, because it is clearly more conspicuous in the $^{13}\text{CO } J=2-1$ and $\text{C}^{17}\text{O } J=3-2$ lines than in the $^{12}\text{CO } J=2-1$ one, which is more opaque, and than in the $^{12}\text{CO } J=3-2$ line, which requires a higher excitation. The fact that the intense maximum is more clearly seen in $^{13}\text{CO } J=2-1$, which is mostly optically thin, strongly suggests that it is due to a condensation, i.e. to that there is a significant increase of the density in those regions. We will discuss in this section the properties and possible origin of this condensation, which could be protoplanetary.

It is remarkable that such strong asymmetries between regions with relatively positive and negative velocity are not frequent in CO-rich rotating disks (Dutrey et al. 2003; Piétu et al. 2005; Simon et al. 2000), even in observations of ^{13}CO lines. An exception may be the C^{18}O maps in DM Tau by Dartois et al. (2003), not their ^{13}CO data, which present an emission excess at certain velocities comparable to that in our ^{13}CO maps. More subtle departures from the keplerian dynamics have been also identified in AB Aur (as well as in our maps of GoHam; see discussion below).

We have tried to estimate how much mass is represented by this excess brightness, although this observational feature is very difficult to model due to the severe lack of information on its nature. A lower limit can be obtained if we assume that the excess mass is just proportional to the total extra intensity in $^{13}\text{CO } J=2-1$. The increase of the line intensity at these velocities represents somewhat less than 20% of the total (velocity integrated) line intensity. Since the total mass of our disk model is $\sim 0.01 M_{\odot}$, we deduce that the mass of the condensation is $\sim 1.5 \cdot 10^{-3} M_{\odot}$, almost identical to the mass of our planetary system or to the mass of Jupiter.

We recall that this mass value must be considered as a lower limit. The excess mass is proportional to the total extra intensity in $^{13}\text{CO } J=2-1$ if this line is completely optically thin and if the excitation in the clump is the same as in the surrounding gas. We know that the first assumption is not completely true even for lines of sight not intersecting the condensation. The second assumption is also improbable, since the density increase must be important and since the opaque $^{12}\text{CO } J=2-1$ line also presents some intensity increase in these regions, suggesting that they are hotter than the corresponding northern regions. The presence of some opacity also in $^{13}\text{CO } J=2-1$ will lead to a perhaps important underestimate of the mass derived from our simple estimate. The effects of the different excitation should be less important. A higher excitation increases the partition function of the molecule and decreases the level population difference, which leads to lower emission in optically thin lines (although, of course, a higher temperature means a higher intensity for high opacities). Therefore, both assumptions will in general lead to underestimates of the clump mass.

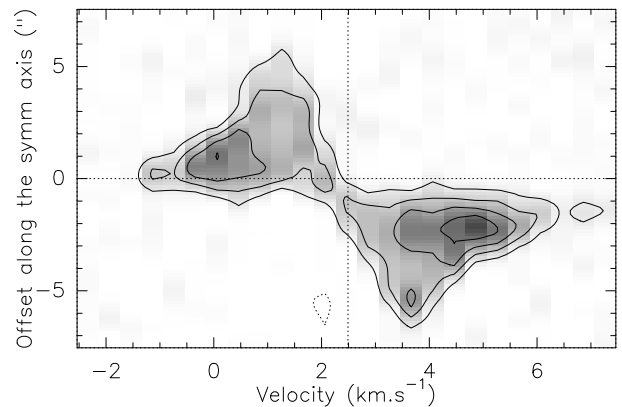


Fig. 8. Position-velocity diagram of the $^{13}\text{CO } J=2-1$ emission from GoHam, obtained along the disk direction (P.A. $=-5^\circ$). The southern emission excess can be seen at positive velocities.

We have performed a better estimate introducing a density increase in some parts of our model disk (destroying the axial symmetry). We have estimated, first, that to model the asymmetry in the $^{12}\text{CO } J=2-1$ maps we need an excess temperature by a factor 1.5 in a southern disk region closer than 10^{16} cm. Then, we have tried to roughly fit the $^{13}\text{CO } J=2-1$ data increasing the density by some factor, with respect to standard law (derived from our fitting of the whole data, Sect. 3, Table 1). A significant factor (~ 10) is found to be necessary to account for the dilution in the beam and some incipient optical depth in this line. The model predictions for the southern brightness increase in $\text{C}^{17}\text{O } J=3-2$ are also compatible with the observations. See a detailed discussion on our tentative modeling of this clump in Sect. A.3. With these conditions, we find that the condensation contains a total mass $\sim 6 \cdot 10^{-3} M_{\odot}$, a few times our planetary system.

We note that these estimates do not exclude the presence of more compact components, not detectable with our angular resolution. We also note that a proto solar system must contain a significantly higher mass than the final planetary system, since significant gas ejection is expected before planets form from such very premature condensations. We also recall that our poor knowledge of the physical properties of these clumps and the poor observational information on it, which practically remains unresolved in our data, prevent any attempt of detailed modeling of the data.

On the other hand, we note that our fitting of the ^{13}CO emission at these velocities is only accurate for the intensity of the clump. In the observations, the brightness maximum appears displaced outwards by 0.5 arcsecond, with respect to the position expected from our fitting (see Appendix). This effect cannot be avoided assuming that the condensation is farther from the star, since then the velocity field we are assuming (the same keplerian law deduced from the fitting of the overall dynamics, Sect. 3) would imply that its emission occurs at too low relative velocities. This displacement can easily be seen in the observations: note the anomalously long distance from the star of the maximum in $^{13}\text{CO } J=2-1$ emission at about 5 km s^{-1} , compared to the brightness distributions at about 3.5 km s^{-1} . Therefore, the presence of a disturbance in the dynamics is necessary to explain the observed properties of the southern condensation, both the disturbance in the dynamics and the condensation being very probably associated.

The standard conditions theoretically required to produce gravitational instabilities in the disk (e.g. Durisen et al. 2007) are not satisfied for this condensation. In GoHam, instabilities would only occur at a less than $\sim 10^{15}$ cm, the distances at which theoretical models tend indeed to predict the presence of protoplanets. The size deduced from our data for the condensation is also too large compared to the Hill sphere, which defines the gravitational domain of a protoplanet (e.g. Lissauer & Stevenson 2007), if we do not assume the presence of undetected compact components. In fact, the mass of the central component required by the large extent of the condensation would be $\sim 0.5 - 1 M_{\odot}$, i.e. that of a low-mass protostar.

From the observational point of view, however, there exists other evidence of the presence of important condensations, probably due to instabilities in the disk, at similar large distances from the star. For instance, the well known spiral structure in AB Aur appears at a distance smaller than about 100 AU or $1.5 \cdot 10^{15}$ cm (Oppenheimer et al. 2008; Millan-Gabet et al. 2006), but spiral-like dust condensations are also detected at several hundred AU (Fukagawa et al. 2004) and seem to have some counterpart in CO emission (Piétu et al. 2005; Lin et al. 2006). Piétu et al. (2005) and Lin et al. (2006) also detected departures from the general keplerian velocity field in the spiral arms of AB Aur, comparable in magnitude to those found by us in GoHam. To better compare our observations with previous results, we represent in Fig. 8 the position-velocity diagram along the disk direction in GoHam, obtained from our $^{13}\text{CO } J=2-1$ data, in which the excess emission is clearly seen at positive velocities. The p-v diagram in GoHam is found to be quite comparable to that obtained by Lin et al. (2006) in AB Aur, in spite of the different angular and velocity scales. The deformation of the dynamics in AB Aur associated with the spiral instability therefore results in a velocity pattern quite similar to that found in Gomez's Hamburger. On the other hand, Lafrenière et al. (2008) have reported the detection, from direct imaging and spectroscopy, of a planet with a mass of about 8 times that of Jupiter at $5 \cdot 10^{15}$ cm from a young star, although systems involving such long distances seem to be rare (Lafrenière et al. 2007). Planets with a few times the mass of Jupiter have been also found around the A-type stars Fomalhaut and HR 8799 (Kalas et al. 2008; Marois et al. 2008), at distances long, ~ 100 AU, though somewhat shorter than that of our condensation. Finally we note the recent detection, from dust emission mapping at 1.3cm wavelength, of a condensation containing 14 times the mass of Jupiter at 65 AU from HL Tau, which was interpreted to be protoplanetary (Greaves et al. 2008).

The southern condensation could also be associated with the presence of a low-mass stellar or quasi-stellar companion, which is able to gravitationally capture a sizeable fraction of the overall disk material and may explain the anomalous dynamics found in the condensation. The contribution of the companion mass ($\lesssim 1 M_{\odot}$) to the total central mass could be necessary to explain that the mass value derived from the overall disk rotation (i.e. derived from data on quite extended regions and regardless of the peculiar kinematics of the condensation) is perhaps too high for the observed total luminosity; see more details above.

In summary, we have identified a condensation in the southern part of the disk, at about $1''.3$ from the disk center, that probably contains a mass of a few times that of Jupiter. This condensation could be protoplanetary, in a very preliminary evolutionary stage; we have noted however that theory predicts that planets tend to form at much smaller distances from the central star, although some observational results support the formation of condensations at such a long distance. This clump could also

be due to material gravitationally captured by a stellar or quasi-stellar companion, whose presence has been independently proposed to explain the total central mass derived from the disk rotation velocity. We recall that the condensation seems to be associated with a significant distortion of the general keplerian velocity field of the bulk of the nebula; this distortion could be explained both if the clump formation is due to the presence of a low-mass stellar companion or to gravitational instabilities within the disk.

Acknowledgements. We are grateful to Asunción Fuente and Mario Tafalla for very helpful comments on the manuscript.

References

- Berne, O., Joblin, C., Fuente, A., & Menard, F. 2008, ArXiv e-prints
 Bujarrabal, V., Castro-Carrizo, A., Alcolea, J., & Neri, R. 2005, *A&A*, 441, 1031
 Bujarrabal, V., Young, K., & Fong, D. 2008, *A&A*, 483, 839 (Paper I)
 Dartois, E., Dutrey, A., & Guilloteau, S. 2003, *A&A*, 399, 773
 Dullemond, C. P., Hollenbach, D., Kamp, I., & D'Alessio, P. 2007, in *Protostars and Planets V*, ed. B. Reipurth, D. Jewitt, & K. Keil, 555–572
 Durisen, R. H., Boss, A. P., Mayer, L., et al. 2007, in *Protostars and Planets V*, ed. B. Reipurth, D. Jewitt, & K. Keil, 607–622
 Dutrey, A., Guilloteau, S., & Guelin, M. 1997, *A&A*, 317, L55
 Dutrey, A., Guilloteau, S., & Ho, P. 2007, in *Protostars and Planets V*, ed. B. Reipurth, D. Jewitt, & K. Keil, 495–506
 Dutrey, A., Guilloteau, S., & Simon, M. 2003, *A&A*, 402, 1003
 Fuente, A., Alonso-Albi, T., Bachiller, R., et al. 2006, *ApJ*, 649, L119
 Fukagawa, M., Hayashi, M., Tamura, M., et al. 2004, *ApJ*, 605, L53
 Greaves, J. S., Richards, A. M. S., Rice, W. K. M., & Muxlow, T. W. B. 2008, *MNRAS*, 391, L74
 Isella, A., Testi, L., Natta, A., et al. 2007, *A&A*, 469, 213
 Jonkheid, B., Dullemond, C. P., Hogerheijde, M. R., & van Dishoeck, E. F. 2007, *A&A*, 463, 203
 Jonkheid, B., Kamp, I., Augereau, J.-C., & van Dishoeck, E. F. 2006, *A&A*, 453, 163
 Kalas, P., Graham, J. R., Chiang, E., et al. 2008, *Science*, 322, 1345
 Lafrenière, D., Doyon, R., Marois, C., et al. 2007, *ApJ*, 670, 1367
 Lafrenière, D., Jayawardhana, R., & van Kerkwijk, M. H. 2008, *ApJ*, 689, L153
 Lin, S.-Y., Ohashi, N., Lim, J., et al. 2006, *ApJ*, 645, 1297
 Lissauer, J. J. & Stevenson, D. J. 2007, in *Protostars and Planets V*, ed. B. Reipurth, D. Jewitt, & K. Keil, 591–606
 Mannings, V. & Sargent, A. I. 1997, *ApJ*, 490, 792
 Mannings, V. & Sargent, A. I. 2000, *ApJ*, 529, 391
 Marois, C., Macintosh, B., Barman, T., et al. 2008, *Science*, 322, 1348
 Millan-Gabet, R., Monnier, J. D., Berger, J.-P., et al. 2006, *ApJ*, 645, L77
 Oppenheimer, B. R., Brenner, D., Hinkley, S., et al. 2008, *ApJ*, 679, 1574
 Panić, O., Hogerheijde, M. R., Wilner, D., & Qi, C. 2008, ArXiv e-prints, 806
 Pety, J., Gueth, F., Guilloteau, S., & Dutrey, A. 2006, *A&A*, 458, 841
 Piétu, V., Guilloteau, S., & Dutrey, A. 2005, *A&A*, 443, 945
 Ruiz, M. T., Blanco, V., Maza, J., et al. 1987, *ApJ*, 316, L21
 Simon, M., Dutrey, A., & Guilloteau, S. 2000, *ApJ*, 545, 1034
 Thi, W.-F., van Zadelhoff, G.-J., & van Dishoeck, E. F. 2004, *A&A*, 425, 955
 van den Ancker, M. E., de Winter, D., & Tjin A Dje, H. R. E. 1998, *A&A*, 330, 145
 Wood, K., Whitney, B. A., Robitaille, T., & Draine, B. T. 2008, *ApJ*, 688, 1118

Appendix A: Selection of the best fitting and accuracy of the parameter values

A.1. Criteria for acceptable models

The general criterion we have chosen to select acceptable models is the comparison of the predicted images with the observed ones. Some authors (e.g. Dutrey et al. 2007; Pety et al. 2006; Isella et al. 2007) perform such a comparison in the Fourier transformed plane of the visibilities. The selected model parameters are then those yielding the smallest residuals, after considering 'blind' variations of the parameter values. Their method has the advantage that is very objective and that uncertainties introduced by the cleaning process are avoided. Other authors

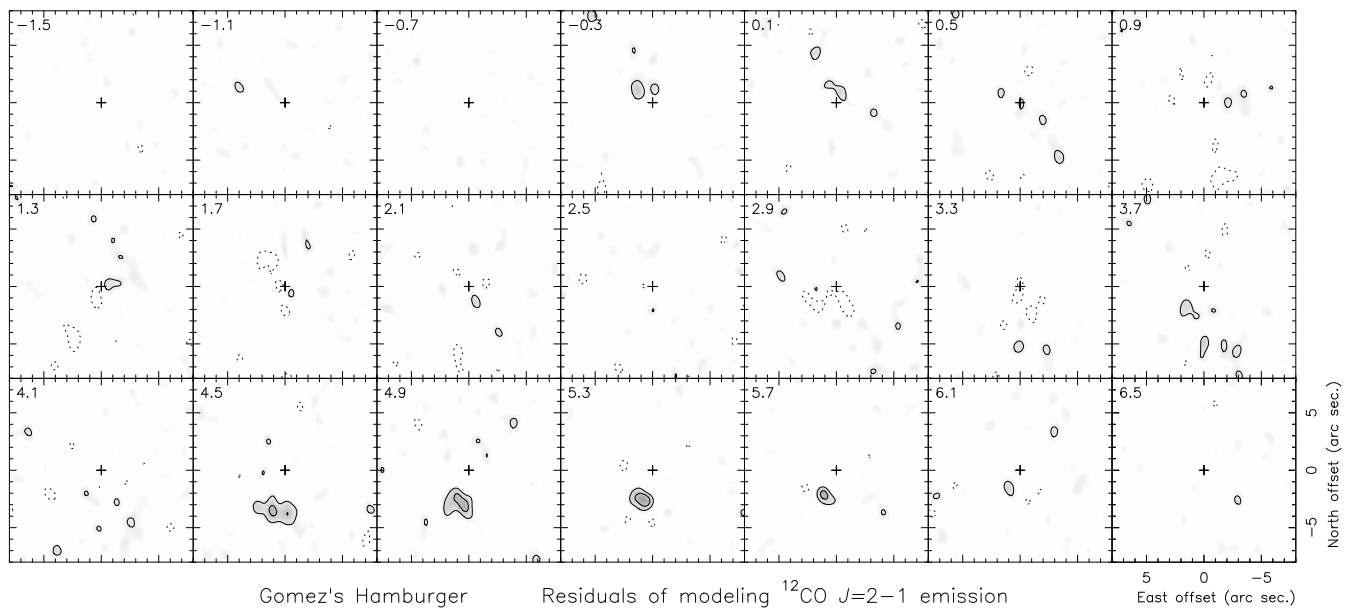


Fig. A.1. Residuals (observations minus synthetic maps) of the $^{12}\text{CO } J=2-1$ line brightness from our best model fitting for the GoHam disk. The spatial scale and contours are the same as in the observations and predictions, Figs. 1, 6.

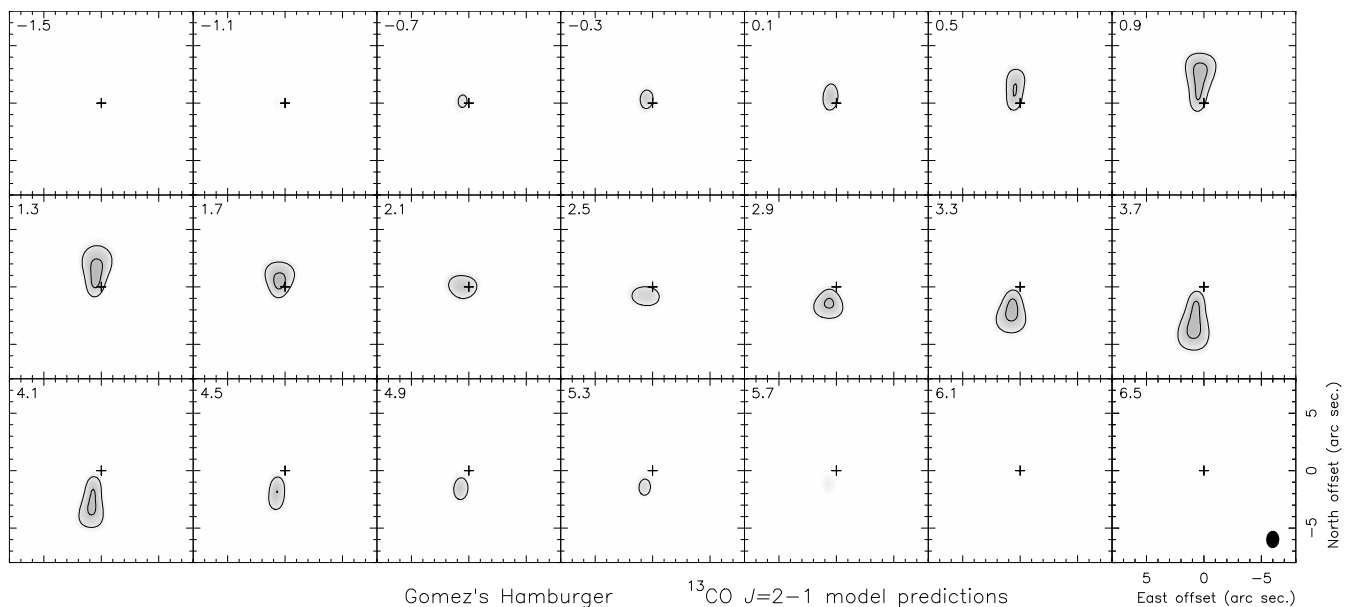


Fig. A.2. Predictions of the $^{13}\text{CO } J=2-1$ line brightness from our best model fitting for the GoHam disk. The spatial scale and contours are the same as in the observations, Fig. 2.

(Mannings & Sargent 1997, 2000; Fuente et al. 2006), follow however a more intuitive approach, directly comparing the images.

In our case, the very high number of free parameters prevents a blind analysis of the resulting residuals for any combination of parameter values, which would imply an exceedingly high amount of calculations. Even the definition of ‘free parameter’ in such a complex structure is difficult, and it is not clear at what extent we can vary all the properties of the disk. Even if theoretical constraints to our model parameters have been widely taken into account (see Sect. 3), we have more than 15 (more or less free) model parameters: 5 defining the geometry, 2 for the dynamics, 5 for the temperature, 3 for the density, plus finally the $^{12}\text{CO}/^{13}\text{CO}/\text{C}^{17}\text{O}$ abundance ratio. It is difficult to decrease such

a large number of parameters in view of the different components identified from the maps: the hotter and less dense fringes separated from the equator, an outer less dense region, the cold central part of the disk, and the central hotter region.

Our procedure, on the other hand, allows an intuitive analysis of the relevance of the different parameters. We can so deduce that some parameters are not relevant to fit some observational properties, and that certain observational features are related to just one or two model parameters. For instance, the total size of the disk is selected to match the total extent of the image, which depends weakly on e.g. the rotational velocity.

It has been argued that in sources comparable in angular size with the telescope resolution the comparison performed in the image plane is not accurate. This is not our case, since GoHam

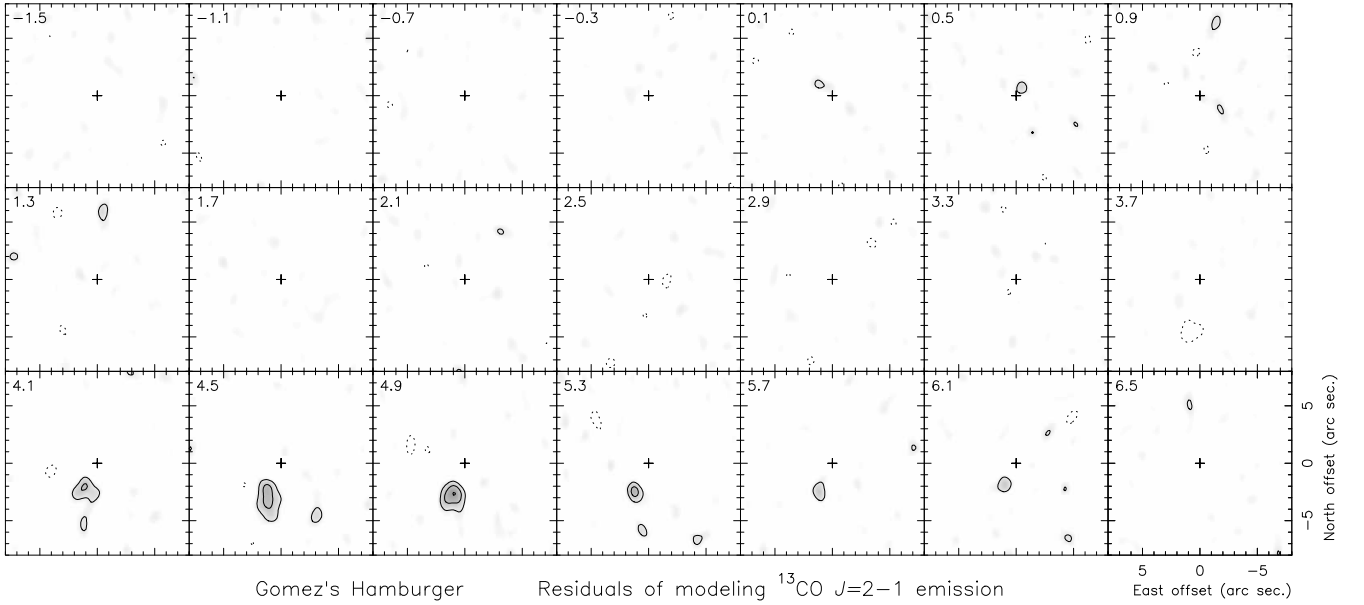


Fig. A.3. Residuals (observations minus synthetic maps) of the $^{13}\text{CO } J=2-1$ line brightness from our best model fitting for the GoHam disk. The spatial scale and contours are the same as in the observations and predictions, Figs. 2, A.2.

occupies about 30 square arcseconds, a surface almost 20 times larger than the beam of our $^{12}\text{CO } J=2-1$ data. The cleaning process always introduces noise, but, besides numerical noise, it is mostly due to uncertainties in the calibration of the complex visibilities, i.e. to that the actual beam shape is not exactly equal to the theoretical beam function (for the uv coverage of the observation). So, subtraction of the convolved ‘clean components’ and the subsequent convolution to get the final image introduces spurious features, mainly when the uv sampling is poor. However, such unavoidable uncertainties in the amplitude and phase calibration appear also if the fitting is performed in the uv plane, and the limitation in the dynamic range of the observations due to them applies to both the sky plane and the Fourier transformed plane. On the other hand, we also note that Fourier transformation of the predicted brightness (which must be calculated for a finite grid of points in space coordinates from the standard radiative transfer equation) also introduces numerical noise.

As we will see below in actual cases, it is practically impossible to define an absolute best fitting model in our case, because of the complex data and model. Instead, we will adopt criteria to consider that a set of parameter values is acceptable and, from cases in which they are not satisfied, will give limits to these values. This process will only be detailed for the most representative parameters: radius and width of the disk, central mass (i.e., rotational velocity law), typical densities and temperatures, ... Among the acceptable models there is no significant difference, both in predictions and in values of the relevant disk properties; one of them has been chosen as our best fit.

To select the acceptable models, we will basically use the comparison of the predictions with the observations of the ^{12}CO and $^{13}\text{CO } J=2-1$ lines, in which the S/N ratio and the spatial and spectral resolutions are particularly high. We have checked that the predictions for the $J=3-2$ lines are also satisfactory. The criteria used to select acceptable models are:

c1) The differential image, i.e. the observed minus synthetic velocity channels, must show in the regions of each channel where emission is present an *rms* noise not exceeding ~ 1.5 times that present in adjacent regions with no emission. Those regions,

with noise not larger than 1.5 times that found in adjacent ones, are only slightly noticeable in the differential maps.

c2) In the differential $J=2-1$ image, the residuals must be smaller than 2 times the spurious contours (due to noise) seen in adjacent regions (~ 0.6 Jy/beam, two contours, in our $^{12}\text{CO } J=2-1$ images), and no residual ≥ 0.3 Jy/beam must appear systematically, i.e. in the same spatial offsets for several velocity channels. We note that in the observed $^{12}\text{CO } J=2-1$ maps one can identify noise features more intense than 0.3 Jy/beam, so residuals not exceeding the above limits are again not clearly different than the observation noise.

These conditions are relaxed for velocities around 4.5–5.5 km s^{-1} LSR, which present a strong emission clump with no counterpart in the equivalent blueshifted emission. This excess cannot be due to opacity or excitation effects, since it is more prominent in the $^{13}\text{CO } J=2-1$ maps than in the $^{12}\text{CO } J=2-1$ ones and much more than for $^{12}\text{CO } J=3-2$. The excess is also clear in the $\text{C}^{17}\text{O } J=3-2$ maps. The fact that this excess is so remarkable in the less optically thick ^{13}CO emission strongly suggests that is mainly due to the presence of a gas condensation, rotating at about 2.5 km s^{-1} at a distance of about $5 \cdot 10^{15}$ cm from the star. Our model shows axial symmetry and therefore cannot explain this excess; we have chosen to mainly fit the emission from the rest of the nebula. A tentative model fitting of this feature is presented in A.3, and the consequences and possible origins of the presence of such a condensation are discussed in Sect. 4.1.

In figure A.1, we present the residuals of our fitting for the $^{12}\text{CO } J=2-1$ maps. Predictions and residuals for $^{13}\text{CO } J=2-1$ are shown in Figs. A.2 and A.3. Except for the velocities around 5 km s^{-1} the typical rms noise out of the emitting regions is of about 0.1 - 0.11 Jy/beam (slightly less for $^{13}\text{CO } J=2-1$), it does not exceed 1.5 - 1.7 Jy/beam in the regions presenting emission. We see that the largest residuals in the differential images do not reach two contours (noise reaching one level is also seen out of the emitting regions).

Of course, between 4.5 and 5.5 km s^{-1} the situation is worse, reflecting the asymmetry in the disk density mentioned above. We can notice some other minor features in the images that are

Table A.1. Relative range of acceptable values, around those given in Table 1, of the main parameters defining the model disk in Gomez’s Hamburger.

Representative parameter	acceptable range	comments
Disk radius	$\times/\div 1.1$	R_{out} and R_{m}
Disk width	$\times/\div 1.1$	H
Keplerian velocity	$\times/\div 1.1$	V_{t}
Temperature High- z jump	$\times/\div 1.1$ between 2 and 5	characteristic value depends on calibration, possible exc. effects (see A.2)
Density Outer disk density	$\times/\div 1.5$ $\times/\div 3$	characteristic value only given by ^{12}CO data, possible exc. effects (A.2)
Turbulent velocity	$\leq 0.1 \text{ km s}^{-1}$	local velocity dispersion
$X(^{12}\text{CO})/X(^{13}\text{CO})$ rel. abundance $X(^{12}\text{CO})/X(\text{C}^{17}\text{O})$ rel. abundance	$\times/\div 1.5$ $\times/\div 2$	

not accounted for by our model: For instance, the ^{13}CO line emission at 3.7 km s^{-1} is less extended than expected, which is not the case at 4.1 km s^{-1} . We also note in our ^{13}CO maps a weak extent towards the north at about 1.3 km s^{-1} , but practically at the noise level. In $^{12}\text{CO } J=2-1$ we see a similar protrusion, but not exactly in the same position. We finally note in some observed panels that the emission from regions close to the star (see e.g. the $^{13}\text{CO } J=2-1$ emission at $\sim 0.5 \text{ km s}^{-1}$ and the ^{12}CO emission at 3.7 km s^{-1}) is somewhat wider than the predictions. The width of our disk is essentially given by the equation of hydrostatics (Sect. 3), under the standard theory of massive flaring disks; it is possible that these usual theoretical requirements are not fully satisfied in the innermost regions of the disks, further analysis of this phenomenon obviously requires higher-quality observations.

A.2. Uncertainty in the fitted parameters

We have estimated the uncertainties in derived values of the model parameters by varying the values for each one (while the others remain unchanged) and checking for which values the above conditions, **c1**, **c2**, are clearly not satisfied. This has been only done for the main, most representative parameters, for instance the radius disk R_{out} , the characteristic density, etc. The results are summarized in Table 1. We also present below some cases in which the uncertainty in the derived parameters requires some discussion.

We have not tried to fully consider the parameter uncertainties when two or more parameters are allowed to vary. For example, the density range is slightly larger than that given in the table if we allow the temperature also to vary, since both variations are in some way compensated. In general, however, the ranges

do not differ very much from our standard uncertainty brackets. The density is mostly fixed by the emission of ^{13}CO and that of $^{12}\text{CO } J=2-1$ from outer regions, while the temperature law is mainly given by the $^{12}\text{CO } J=2-1$ and $J=3-2$ maps.

We note the uncertain determination of the density in the outer disk ($r \sim R_{\text{out}}$), which is only given by the ^{12}CO emission, since ^{13}CO is not detected in this region; see Table A.1. We also recall that the assumption of level population thermalization may not be valid for these diffuse regions, which may imply that the density in them is somewhat larger than the values given here, perhaps closer to $3 \cdot 10^3 \text{ cm}^{-3}$.

Important problems with the thermalization assumption are not expected for the relatively high densities of the rest of the nebula and the analyzed transitions (Sect. 3). The $J=6-5$ transition is significantly more sensitive to these effects, due to the relatively high Einstein coefficients of high- J transitions. We also expect underpopulation of the $J=6$ and $J=5$ levels in the high- z low-density regions, with $n \sim 10^4 \text{ cm}^{-3}$, leading to 6-5 brightness temperatures under 10 K. This line would mainly come from this high-temperature surface, and we think that this phenomenon is in fact the responsible for the non-detection of $^{12}\text{CO } J=6-5$ in our observations. Any further discussion is not justified in view of the lack of accurate information on the $J=6-5$ emission. This relative underpopulation of high- J levels in the layers at high absolute values of z may lead to a relative overpopulation of the $J=2$ level, and therefore to more emission than expected in $J=2-1$. This effect could lead to slightly smaller jumps of the temperature, perhaps closer to factor 2.

Some parameter pairs are quite dependent one on the other. This is in particular the case of the density and the CO total abundance, since we are assuming LTE and the line opacity depends on the product of the density and the relative abundance. So both parameters can freely vary, provided that their product

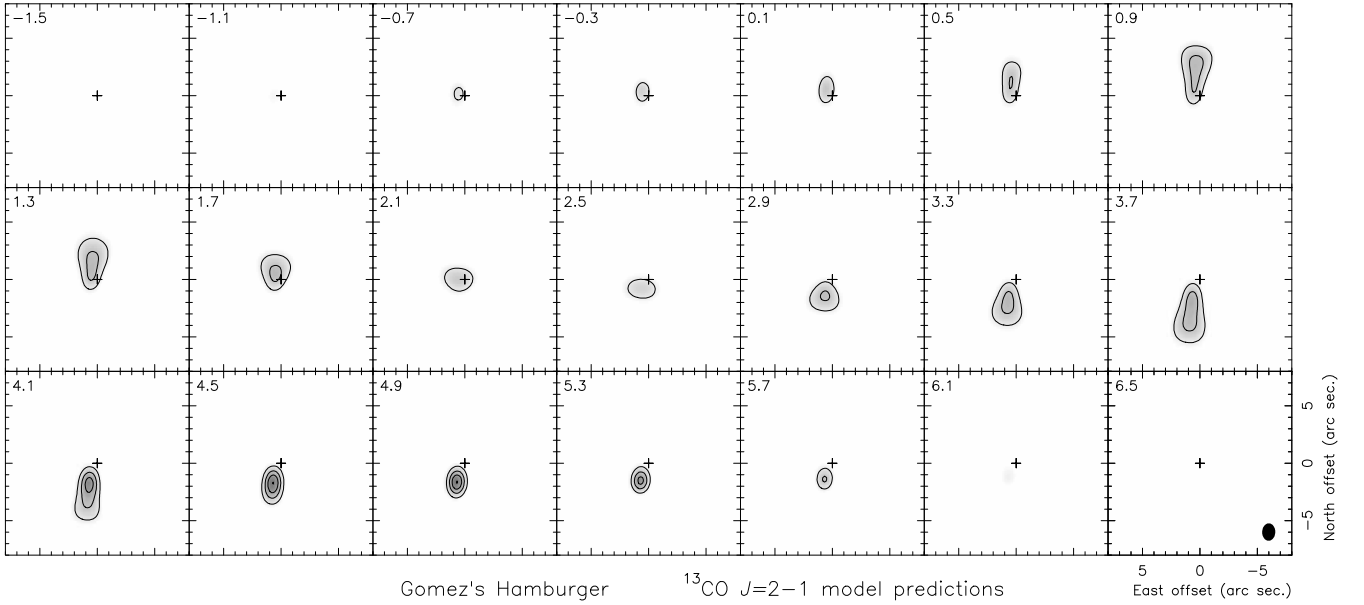


Fig. A.4. Predictions of the $^{13}\text{CO } J=2-1$ line brightness from our best model fitting for the GoHam disk, including the increase in temperature and density in a southern clump, as described in App. A.3. The spatial scale and contours are the same as in the observations, Fig. 2, and our standard model predictions, Fig. A.2.

is kept constant. The indetermination is solved assuming a relative ^{12}CO abundance of 10^{-4} . This is also the case of parameters that we have not considered separately in this uncertainty analysis, like the temperature at a given point, $T(R_0)$, and the slope of the temperature law, α_T ; instead, as mentioned, we just discuss the uncertainty in the characteristic temperature. Finally, we note the case of the rotation velocity and the conditions in the hot and dense center of the disk. A strong emission from these regions may mimic the emission of a faster rotating disk in the extreme velocity channels. So, the rotation velocity is mainly determined from the emission extent in the channels at moderate velocities, the emission at the extreme channels depending on both the keplerian velocity and the emissivity of the central regions. In general, the uncertainty of the parameters defining the inner, denser region ($r < 2 \times R_{\text{in}}$) is high, because this clump is not resolved and the number of independent observational constraints is small (as also concluded in Paper I). We can say that an inner region with higher density and temperature is necessary to attain our strong requirements to the fitting quality and that it must be smaller than about 10^{16} cm; but we cannot give details on this region.

The outer hot region, for high values of z , is hardly resolved in our ^{12}CO maps. Therefore, we could also fit our data assuming that this region is significantly thinner and brighter (in general, hotter) than in our standard model. We think however that those disk models are less probable than our standard ones, because our standard jump in temperature is already quite high (see Sect. 3). Moreover, for very high temperatures in the high- z rim, we should also increase significantly the typical density (to fit $^{12}\text{CO } J=2-1$, which, for the assumed dependence of the density with z , is only moderately opaque in the high- z regions). This would then imply too low values of $X(^{13}\text{CO})$, to fit $^{13}\text{CO } J=2-1$, leading to improbably high values of $X(^{12}\text{CO})/X(^{13}\text{CO})$, significantly over 100. In any case, we note that the properties of this high- z bright rim vary only moderately with its temperature (because of the moderate opacity in $^{12}\text{CO } J=2-1$) and depend on the relative calibration of the $J=2-1$ and $J=3-2$ lines; allowing 15% variations in the relative calibrations, we can fit the data with temper-

ature jumps ranging between 2 and 5 (and hot-layer widths not very different from our standard value).

A.3. Model (tentative) fitting of the southern brightness maximum

We have mentioned that there is a relative maximum in the southern part of the disk that has no counterpart in the north. This maximum is seen in all our maps, but it is more prominent in ^{13}CO emission, which is mostly optically thin, as well as in the C^{17}O line. Therefore, this brightness maximum must be mainly due to an increase of the density in some southern regions, though some increase in temperature is also necessary to explain the excess observed in $^{12}\text{CO } J=2-1$.

In our standard model analysis, we have mostly tried to fit the emission from the rest of the nebula (Sects. 3, A1, A2). Any attempt to fit the emission excess from this southern clump is very uncertain, because of the lack of previous experience trying to study condensations of this kind, including the lack of theoretical modeling, and because of the poor information contained in our observations, which scarcely resolve its extent.

Nevertheless, we note that this emission excess can be detected over a remarkable range of velocities, between about 4.1 and 5.7 km s^{-1} LSR. This means that the emitting condensation cannot be very small, the projected velocity dispersion being due to gas emitting from different distances from the star or from regions showing a significant variation of the projection of the velocity on the line of sight. In both cases, we expect typical sizes $\sim 5 \cdot 10^{15}$ cm ($\sim 1''$ for the adopted distance). We can also assume that the condensation takes place in the equatorial disk regions from which $^{13}\text{CO } J=2-1$ emission comes, because the maximum is so prominent in this line. We have assumed that the emission comes from region defined by $R_{\text{in}} < r < 10^{16}$ cm, and $z_s/r < 0.6$, where z_s is the distance between a given point and the plane containing the star and perpendicular to the equator that gives the extreme projections for the rotation velocity. We assume that the temperature and density of this region vary with respect to the standard laws assumed for the rest of the nebula.

We have estimated that, to explain the (moderate) emission excess found in $^{12}\text{CO } J=2-1$, we must assume an increase in temperature in the southern condensation by a factor ~ 1.5 , with respect to our standard laws for nearby regions. Finally, we have estimated the excess density in the condensation by comparison of the model results with the intensity of the $^{13}\text{CO } J=2-1$. Since the $^{13}\text{CO } J=2-1$ emission from these inner regions is not fully optically thin, a significant density increase, by a factor 10, is necessary. A total mass increase of about $6 \cdot 10^{-3} M_{\odot}$ is deduced.

The resulting brightness distribution is shown in Fig. A.4. We can see that the brightness excess of $^{13}\text{CO } J=2-1$ in this southern clump is reasonably well reproduced, but the location of the predicted maximum is slightly closer to the star than the observed one. This cannot be avoided assuming a longer distance from the star for the clump, because then the velocity of the feature would be less positive. The velocity field in this region must then be also disturbed. See discussion on the interpretation of this emission excess in Sect. 4.1.